Cell Reports

Resource

An Inducible Lentiviral Guide RNA Platform Enables the Identification of Tumor-Essential Genes and Tumor-Promoting Mutations In Vivo

Graphical Abstract

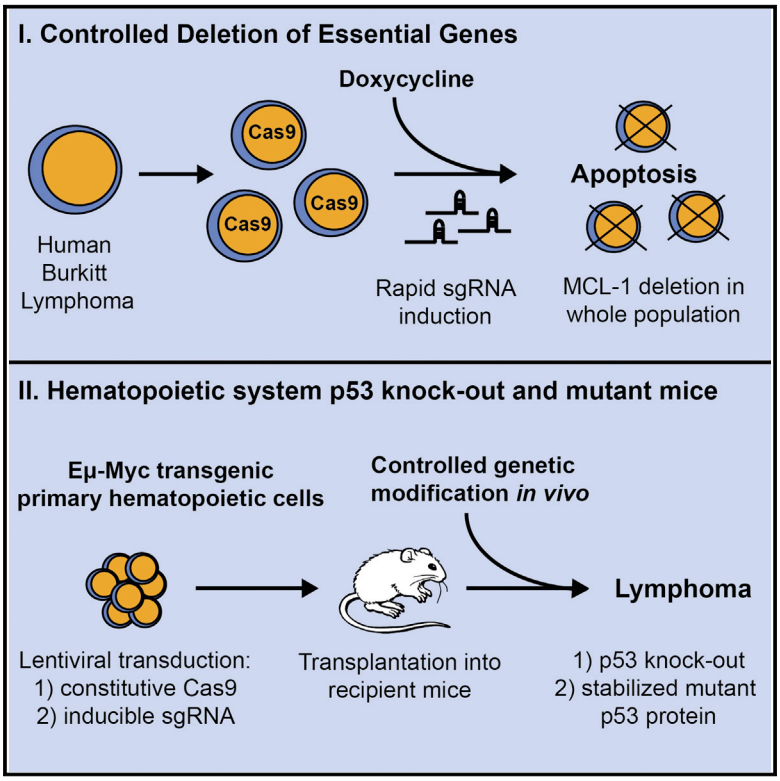

Highlights

- A lentiviral CRISPR/Cas9 platform for the conditional targeting of essential genes
- Efficient mutation of genes in mouse and human cell lines and primary mouse cells
- Identification of cancer-promoting mutations in the tumor suppressor p53

Authors

Brandon J. Aubrey, Gemma L. Kelly, ..., Andreas Strasser, Marco J. Herold

Correspondence

herold@wehi.edu.au

In Brief

The CRISPR/Cas9 system is an exciting methodology for genetic modification. Aubrey et al. have advanced this technology by developing an inducible lentiviral system. This platform facilitates efficient gene targeting that permits phenotypic assessment following deletion of essential genes and identification of tumor-promoting mutations in vivo.

Aubrey et al., 2015, Cell Reports *10*, 1422–1432
March 3, 2015
http://dx.doi.org/10.1016/j.celrep.2015.02.002

CellPress

OPEN ACCESS
CellPress

Cell Reports
Resource

An Inducible Lentiviral Guide RNA Platform Enables the Identification of Tumor-Essential Genes and Tumor-Promoting Mutations In Vivo

Brandon J. Aubrey,[1,2,3,4] Gemma L. Kelly,[1,2,4] Andrew J. Kueh,[1,2] Margs S. Brennan,[1,2] Liam O'Connor,[1,2] Liz Milla,[1,2] Stephen Wilcox,[1,2] Lin Tai,[1] Andreas Strasser,[1,2] and Marco J. Herold[1,2,*]

[1]Walter and Eliza Hall Institute of Medical Research, Parkville, VIC 3052, Australia
[2]Department of Medical Biology, University of Melbourne, Parkville, VIC 3050, Australia
[3]Department of Clinical Haematology and Bone Marrow Transplant Service, the Royal Melbourne Hospital, Parkville, VIC 3050, Australia
[4]Co-first author
*Correspondence: herold@wehi.edu.au
http://dx.doi.org/10.1016/j.celrep.2015.02.002

SUMMARY

The CRISPR/Cas9 technology enables the introduction of genomic alterations into almost any organism; however, systems for efficient and inducible gene modification have been lacking, especially for deletion of essential genes. Here, we describe a drug-inducible small guide RNA (sgRNA) vector system allowing for ubiquitous and efficient gene deletion in murine and human cells. This system mediates the efficient, temporally controlled deletion of MCL-1, both in vitro and in vivo, in human Burkitt lymphoma cell lines that require this anti-apoptotic BCL-2 protein for sustained survival and growth. Unexpectedly, repeated induction of the same sgRNA generated similar inactivating mutations in the human *Mcl-1* gene due to low mutation variability exerted by the accompanying non-homologous end-joining (NHEJ) process. Finally, we were able to generate hematopoietic cell compartment-restricted *Trp53*-knockout mice, leading to the identification of cancer-promoting mutants of this critical tumor suppressor.

INTRODUCTION

The manipulation of genes of interest has been vital for deciphering the roles of many signal transducers, regulators of gene expression, and structural components within a cell or an entire organism. While ectopic expression of genes in cell lines or primary cells has been readily achievable for several decades, the ablation of genes (and their products) has been a considerably harder task, especially in species other than the mouse. Initial attempts to suppress gene expression included RNA antisense technology (Mizuno et al., 1984), but this has not proven to be very robust or efficient. The discovery of RNAi improved the targeting methodology and made it for the first time possible to knock down the expression of genes in cells of several species in vitro as well as in vivo (Fire et al., 1998; Sontheimer, 2005). However, the levels of certain gene products could only be reduced to a minor extent or not at all; this was particularly the case for genes that are essential for the sustained growth of cells (Ottina et al., 2012). A plethora of new genome-editing technologies, such as zinc-finger nucleases (ZFNs) or transcription activator-like nucleases (TALENs), have paved the way to overcome these hurdles. With these technologies, it became possible to generate targeted gene mutations and knockouts in cell lines of different species and even whole organisms by directly mutating the genome rather than by degrading mRNA products. Although more robust, the complex nature of generating ZNFs and TALENs makes the routine use of this methodology challenging. The recently developed CRISPR/Cas9 genome-editing technology with its high efficiency, ease, speed, and therefore relatively low expenditure now appears to replace ZNFs and TALENs to become the method of choice in many laboratories.

Clustered, regularly interspaced, short palindromic repeats (CRISPRs) and the Cas9 endonuclease have been adapted from their normal role in bacterial and archaean defense against phage infections (Barrangou et al., 2007; Wiedenheft et al., 2012) for the rapid editing of eukaryotic genomes (Cong et al., 2013; Mali et al., 2013; Pennisi, 2013). The system utilizes the DNA-cleaving capacity of the *Streptococcus pyogenes* Cas9 endonuclease, which can be directed to specific DNA sequences in virtually any genome by an engineered small guide RNA (sgRNA) (Jinek et al., 2012). The resultant sites of DNA cleavage are repaired by non-homologous end-joining (NHEJ). This DNA repair mechanism introduces random mutations into the targeted gene at high frequency, resulting in its functional inactivation (Jinek et al., 2012). The Cas9 endonuclease requires sgRNA-mediated conformational activation to facilitate DNA binding and cleavage (Jinek et al., 2014).

Despite the advantages offered by CRISPR/Cas9-mediated gene inactivation, several technical problems impede its use in many experimental settings. Current tools for Cas9-mediated genome editing still require subsequent phenotypic or genetic screening and usually necessitate selection for relatively rare modified cells. This does not allow for the targeting of essential genes that may render cells non-viable. Furthermore, with existing CRISPR/Cas9 methodologies, the overall efficiency of NHEJ

repair within a bulk population of cells is too low to evaluate the functional consequences of gene inactivation.

To overcome these issues, we sought to improve upon existing CRISPR/Cas9 techniques to make the system (1) more efficient, (2) applicable to a broader spectrum of cell types, and (3) temporally controllable. To this end, we engineered a lentiviral vector platform that allows for efficient transduction of cells and subsequent inducible expression of sgRNAs with concomitant constitutive expression of Cas9. We validated the efficiency of this new platform in human and mouse cell lines in vitro by knocking out the pro-apoptotic BH3-only protein BIM. In order to demonstrate the ability of the system to efficiently target genes that are essential for sustained cell growth, we conditionally deleted *Mcl-1* in human Burkitt lymphoma (BL) cells, which are highly dependent on this anti-apoptotic BCL-2 family member for their survival (Kelly et al., 2014). Upon induction of the *Mcl-1* sgRNA, these cells were killed at a very high frequency, and this correlated with the number of InDels (insertions and deletions of bases in the DNA) introduced into the *Mcl-1* locus by the NHEJ machinery. Interestingly, when applying a newly developed next-generation sequencing pipeline, we found that the frequency and nature of InDels induced by individual sgRNAs were highly similar to each other, suggesting that the CRISPR/Cas9-induced NHEJ process is not as random as originally envisaged. Finally, we used our system to generate hematopoietic-cell-restricted *Trp53*-knockout mice through the introduction of constitutive Cas9 and inducible *Trp53* sgRNAs into hematopoietic stem/progenitor cells (HSPCs) that were then transplanted into myelo-ablated recipient mice. Interestingly, we generated not only mutations that caused loss of the TRP53 protein but also novel mutant TRP53 proteins that could promote lymphoma development. This shows that our highly efficient inducible CRISPR/Cas9 platform can be used to identify novel gene mutations that drive tumorigenesis.

RESULTS

Establishment of an Inducible Lentiviral Guide RNA Expression System

In order to obtain highly efficient gene-knockout rates in difficult-to-target mouse and human cell lines and primary cells, we developed a dual lentiviral vector system consisting of (1) a constitutive expression vector for the Cas9 endonuclease linked via the T2A peptide to the mCherry fluorescent marker protein and (2) a doxycycline (dox)-inducible sgRNA cassette and ubiquitin promoter driven tetracycline (Tet) repressor linked via the T2A peptide to the GFP protein (Figure 1A). The sgRNA is driven by the H1 promoter, which permits any start base in the sgRNA sequence and hence facilitates increased coverage of potential guide RNA targeting sites within the mammalian genome (Ranganathan et al., 2014). Additionally, the H1 promoter contains a Tet-operator site, allowing for tight suppression of the promoter activity in the presence of a codon-optimized Tet repressor, which can be rapidly and efficiently relieved by the addition of dox (Herold et al., 2008). We first validated the activity of the viral vectors in human 293T cells using sgRNAs targeting exon 2 or exon 3 in the genomic locus of the human pro-apoptotic BCL-2 family member *Bim*. Induction of *Bim* sgRNAs with dox led to efficient loss of BIM protein (Figure 1B). DNA sequence analysis of (non-clonal) cell pools confirmed the modification of the *Bim* locus (Figure 1C). We next attempted the knockout of *Bim* in the murine factor-dependent cell progenitor-1 (FDC-P1) myeloid progenitor cell line. To this end, we transduced FDC-P1 cells that stably express Cas9 with dox-inducible sgRNA vectors targeting exon 2 or exon 3 of the genomic locus of the murine *Bim* gene (*isgBim_muEx2 or isgBim_muEx3*). Addition of dox caused a prominent reduction of BIM protein within the whole population (Figure 1D). We then generated single-cell clones from the dox-induced FDC-P1 *isgBim*-knockout populations to investigate the frequency of loss of the BIM protein and its molecular basis. Remarkably, 19 out of 20 clones derived from the parental cell populations transduced with either of the two sgRNAs targeting *Bim* showed no residual BIM protein expression, demonstrating the high efficiency of our lentiviral-based inducible CRISPR/Cas9 system (Figure 1E). DNA sequence analysis of the *Bim*-targeted FDC-P1 clones confirmed the presence of mutations in the target sequence (Figure 1F). Remarkably, mutations such as a T insertion leading to a premature stop codon in the *Bim* mRNA were repeatedly observed in different clones and also in CRISPR/Cas9-generated BIM-deficient mice using the same sgRNA (Figure 1F; data not shown).

We also compared the efficiency of a dox-inducible Cas9 lentiviral vector with our dox-inducible sgRNA system. To this end, we transduced 293T cells with inducible Cas9 and constitutive *sgBim_huEx2*. Addition of dox to the inducible Cas9/*sgBim*-transduced cells resulted in no detectable reduction of the BIM protein, while *isgBim_huEx2* with constitutive Cas9 showed a strong reduction in BIM protein levels (Figure S1A). Although both cell populations were transduced at similar frequencies with the constitutive and inducible Cas9 expression constructs (Figure S1B), Cas9 protein levels expressed from the inducible vector did not reach the same level as in the constitutive expression setting, even after 72 hr of dox treatment (Figure S1A). This probably explains the lower targeting efficiency observed with inducible Cas9. To further compare the inducible Cas9 system with our inducible sgRNA configuration, we established FDC-P1 cell lines expressing inducible or constitutive Cas9 in combination with constitutive or inducible sgRNAs, respectively, targeting exon 2 and exon 3 of the mouse *Bim* gene. Western blot analysis confirmed the results obtained in the 293T cells with almost no lowering of BIM protein using the inducible Cas9 but highly efficient reduction of BIM protein using the inducible sgRNA system (Figure S1C). In order to quantify and compare the InDel formation between the inducible Cas9 and inducible sgRNA system, we established a next-generation sequencing protocol (Figure S1D). We isolated genomic DNA from the FDC-P1 cell lines and amplified ~250 bp of the sgRNA-targeted genomic region using chimeric oligonucleotides (oligos) consisting of gene-specific and common sequences. The use of the common sequences allows for the amplification of the region in a secondary PCR reaction that incorporates bar-coded oligos as sample identifiers. The incorporation of differently bar coded forward and reverse primers and their applicability to any modified gene reduces the number of oligos needed by up to ~80%. Importantly, while both systems showed minimal InDel formation in steady state, dox treatment resulted in 60%–80% mutation

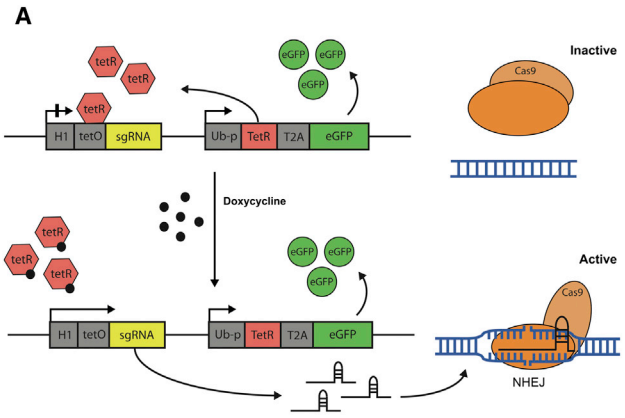

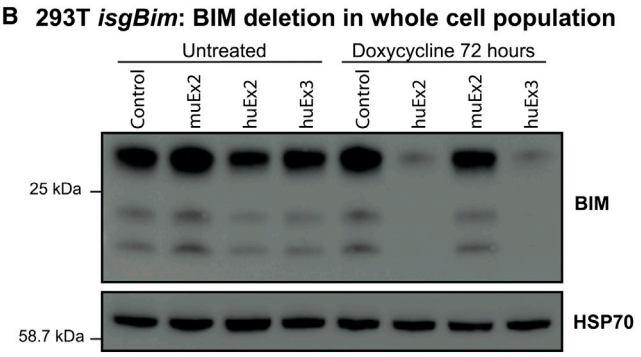

C 293T cell line targeted InDels: *isBim_huEx2*

---CCTGCGGAGAGGCCTCCCCAGCTCAGACCTGGGGCCCCTACCTCCC---	*wild-type reference*
---CCTGCGGAGAGGCCTCCCCAGCTCAGAC -TGGGGCCCCTACCTCCC---	293T Bim #1
---CCTGCGGAGAGGCC----------(-25bp)----------ACCTCCC---	293T Bim #2
---CCTGCGGAGAGGCCTCCCCAGCTCAGGTA -GGGGCCCCTACCTCCC---	293T Bim #3

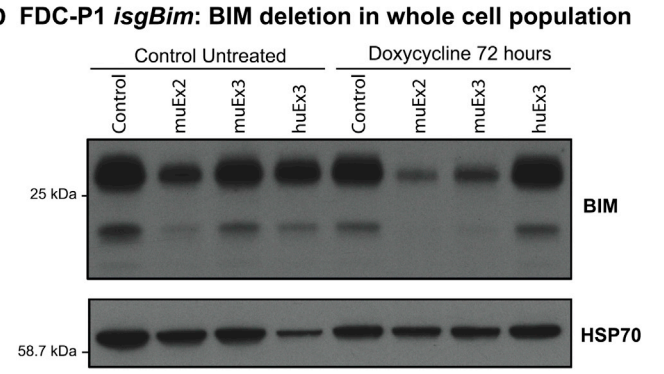

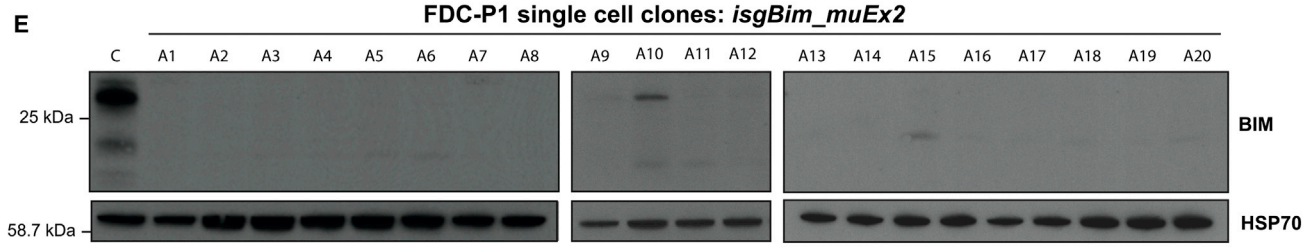

F

sequence	FDC-P1 (n=6)	primary mouse (n=13)
WT ---AGAGAAGGTGGACAATTGCAGCCTGCT - -GAGAGGCCTCCCC---	-	x2 alleles
---AGAGAAGGTGGACAATTGCAGCCTGCT -TGAGAGGCCTCCCC---	**x8 alleles**	**x11 alleles**
---AGAGAAGGTGGACAATTGCAGCCTGCTCTGAGAGGCCTCCCC---	x2 alleles	-
5 base pair deletion	-	x1 allele
9 base pair deletion	-	x1 allele
17 base pair deletion	-	x5 alleles
21 base pair deletion	-	x2 alleles
24 base pair deletion	x1 allele	x1 allele
27 base pair deletion	-	x3 alleles
213 base pair insertion	x1 allele	-

Figure 1. Establishment and Validation of the Inducible Guide RNA Platform

(A) Schematic for doxycycline (dox)-inducible guide RNA lentiviral vectors. Cas9 is constitutively expressed in the cells. Treatment with dox rapidly induces the sgRNA, which activates Cas9 and directs it to the target genomic sequence.

(B) Targeting of *Bim* in human 293T cells using human *isgBim_huEx2* (huEx2) and human *isgBim_huEx3* (huEx3); *mouse isgBim_muEx2* (muEx2) was used as a negative control. Western blotting for human BIM with probing for HSP70 used as a loading control in a whole population of 293T cells transduced with constitutively expressed Cas9 and dox-inducible sgRNA lentiviral vectors before and after treatment with dox (1 μg/ml).

(C) Conventional Sanger DNA sequencing analysis to confirm the presence of InDel mutations at the target site for the *Bim*-sgRNA. Representative examples are shown with reference wild-type sequence in the first line. The sgRNA binding site is shown in green, and InDel mutations are shown in purple.

(D) Targeting of *Bim* in a whole population of mouse FDC-P1 cells before and after treatment with dox using mouse *isgBim_muEx2* (muEx2) and mouse *isgBim_muEx3* (muEx3); human *isgBim_huEx3* (huEx3) was used as a negative control. Western blotting for mouse BIM with probing for HSP70 used as a loading control.

(E) Efficiency of *Bim* targeting in 20 single-cell-derived clonal populations of *Bim*-targeted FDC-P1 cells (numbered A1–A20). Western blotting for mouse BIM with probing for HSP70 used as a loading control.

(legend continued on next page)

rates using the inducible sgRNA as compared to only 5%–10% for the inducible Cas9 (Figure S1E). This demonstrated that the inducible sgRNA exerted a more robust effect, and this is likely due to the ubiquitous and strong activity of the inducible H1 promoter as well as the faster kinetics for transcribing a small RNA as compared to producing the large Cas9 protein endonuclease (Ranganathan et al., 2014).

Collectively, these results demonstrate that our new inducible lentiviral CRISPR/Cas9 platform can be used to efficiently delete genes in murine and human cell lines.

Analysis of the Consequences of BIM Deletion in Human BL-Derived Cell Lines

In order to test the applicability of the lentiviral platform in human hematopoietic cell lines and to assess phenotypic consequences of the targeting of a specific gene, we introduced *isgBim_huEx3* into the human BL-derived cell lines Rael-BL (Figure 2) and Kem-BL (Figure S2). Due to the inducibility of our vector system, whole or single-cell clonal populations could be established by fluorescence-activated cell sorting (FACS) based on mCherry and eGFP expression (Figure 2A), prior to sgRNA induction with dox. This strategy optimizes the efficiency of gene targeting throughout the population of cells after expression of the sgRNA is induced. Loss of BIM protein in the Rael-BL cell line (Figure 2B) correlated with resistance to the calcium ionophore ionomycin (Figure 2C), a cytotoxic insult known to induce apoptosis in a BIM-dependent manner (Bouillet et al., 1999). As expected, we detected InDel mutations with high frequency in exon 3 of the *Bim* locus using the NGS platform (Figures 2D and S2B).

These results show that the inducible *sgRNA* lentiviral platform facilitates efficient deletion of the pro-apoptotic BCL-2 family member *Bim* in human hematopoietic lymphoma cell lines and that this leads to functional inactivation of the BIM protein.

Inducible Deletion of MCL-1 in Human BL-Derived Cell Lines and Its Functional Consequences

It is conceptually easier to obtain cells bearing mutations in pro-apoptotic genes (e.g., *Bim*) than in genes that are essential for cell survival. Therefore, having established the high efficiency of our new platform for introducing the desired mutations, we sought to inactivate the *Mcl-1* gene in BL cell lines, which require this anti-apoptotic BCL-2 family member for sustained survival (Kelly et al., 2014). To confirm the efficacy of the sgRNA targeting *Mcl-1*, we first used the Sal-BL cell line that can grow independent of MCL-1 due to the expression of the EBV-encoded anti-apoptotic BCL-2 homolog BHRF-1 (Kelly et al., 2002). MCL-1 protein loss could be readily achieved in this cell line (Figure S3A) and, as expected, did not cause loss of viability (data not shown). Next, we turned to Rael-BL cells, which require MCL-1 for survival (Kelly et al., 2014). Rael-BL cells were stably transduced with Cas9 and two independent inducible sgRNAs targeting different regions of the human *Mcl-1* gene. Single-cell clones were generated by FACS (mCherry/eGFP double-positive cells) to obtain cell populations that uniformly express Cas9 (reported by mCherry) and also contain the inducible *Mcl-1*-targeting sgRNA (reported by the constitutively expressed eGFP). Induction of either of the two *Mcl-1*-targeting sgRNAs by dox efficiently induced apoptosis (up to 75%) in the majority of the single-cell-cloned lines tested (Figure 3A). As expected, the loss of MCL-1 protein, as measured by western blotting, correlated with the extent of apoptosis induction observed in these cells (Figure 3B). Because the sgRNA vector is dox inducible, we could assess the induction of apoptosis, NHEJ efficiency, and the pattern of InDel mutations from multiple discrete experiments. Repeated induction of the sgRNAs targeting *Mcl-1* in the single-cell-cloned populations resulted in similar reductions in MCL-1 protein and a similar extent of apoptosis (Figure 3A). Furthermore, the frequency of InDels generated upon dox induction in the MCL-1-dependent clonal cell lines correlated strongly with the extent of cell death; i.e., ~60% InDel mutations corresponded to 60%–70% cell killing (Figure 3C). Strikingly, we detected the generation of similar InDel mutations by the *Mcl-1*-specific guide RNAs in different experiments and different clonal cell populations (Figures 3D, S3B, and S3C). These results demonstrate that the NHEJ process induced by the CRISPR/Cas9 system is not as random as envisaged, and it will be interesting to explore the factors that determine this selectivity.

Next, we wanted to test, whether targeting of MCL-1 with our inducible CRISPR/Cas9 platform would also be usable to impede tumor growth in vivo. To this end we subcutaneously injected a variety of the engineered *isgMcl-1* BL populations into immune-deficient non-obese diabetic/severe combined immunodeficiency (NOD/SCID) common-γ chain knockout (NSG) mice. We used populations, which upon induction of the *Mcl-1* specific guide RNAs in vitro were either killed (responders) or stayed alive (non-responders). In addition, prior to transplantation into the NSG mice, these BL lines were transduced with a luciferase expression vector to allow for monitoring of tumor progression in vivo using bioluminescent imaging. After 21 days, successful engraftment was assessed using bioluminescent imaging and mice bearing tumors were commenced on dox-containing food to induce the expression of the *Mcl-1*-specific sgRNA. Excitingly, 5 days following dox treatment, we observed dramatic tumor regression (37.5%) or impaired growth (62.5%) in mice transplanted with responder cells, as compared to dox-treated mice carrying non-responder cells (Figures 3E and S3D), which all displayed marked tumor progression. Importantly, these experiments demonstrate that our lentiviral CRISPR/Cas9 system works highly efficiently in vivo under temporal control and that CRISPR/Cas9-mediated genome editing may be used as a novel approach to anti-cancer therapy.

In order to further determine (1) the tightness of our system and (2) the time at which the first InDels can be detected, we analyzed InDel formation in the *Mcl-1* locus from 0 to 72 hr following dox application (Figure S3E). Interestingly, InDel formation was

(F) Conventional Sanger DNA sequencing analysis to confirm targeting of the mouse *Bim* locus in clonal FDC-P1 cell lines as well as CRISPR/Cas9-generated *Bim* mutant mice. DNA sequencing demonstrated a frequently re-occurring T insertion. Results are shown for six single-cell-cloned lines (i.e., 12 *Bim* alleles) with all clones demonstrating homozygous mutated alleles. Comparison is made to DNA sequencing results from CRISPR/Cas9-generated mutant mice (n = 13) that also displayed reoccurring T insertion. The sgRNA binding site is shown in green, and mutations are shown in purple.

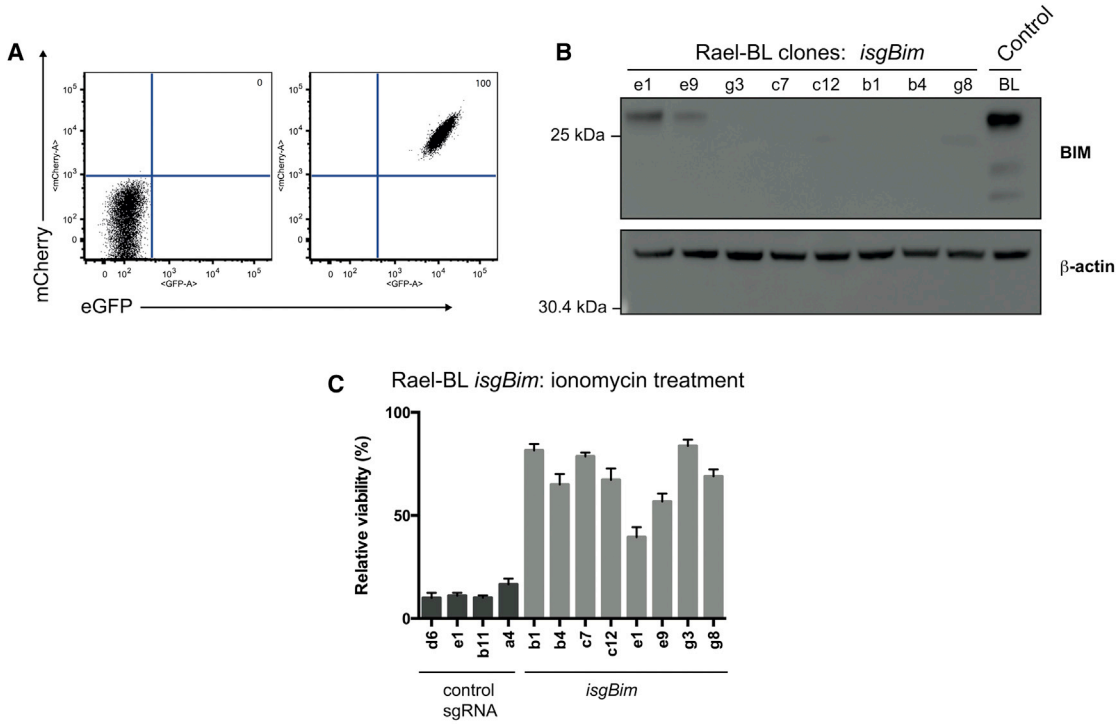

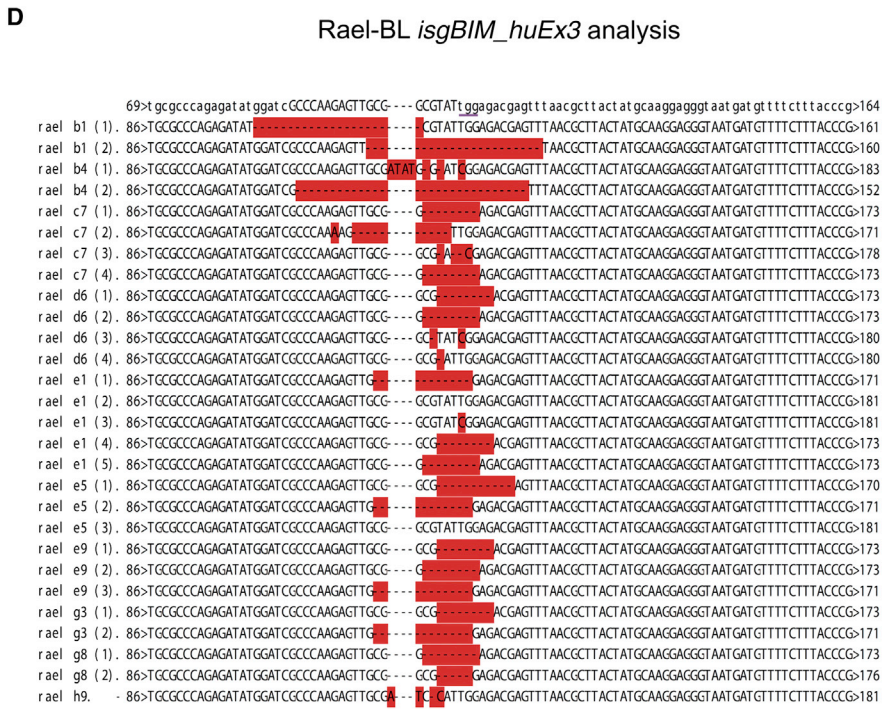

Figure 2. BIM Deletion in Human BL Cell Lines and Next-Generation Sequencing Platform

(A) Representative example of a Rael Burkitt lymphoma (BL) single-cell clonal line obtained by FACS that uniformly expresses Cas9 (reported by mCherry) and also uniformly contains the inducible sgRNA vector (marked by constitutively expressed eGFP).

(B) Western blotting for BIM (probing for β-actin used as a loading control) demonstrates loss of BIM following dox-mediated induction of the *isgBim* in a bulk population of Rael-BL single-cell-derived clonal lines.

(legend continued on next page)

peaking between 48 and 72 hr, while prior to dox treatment, almost no InDels could be detected. Accordingly, this correlated nicely with minimal sgRNA expression before and strong induction (up to 700-fold increase) after dox treatment peaking between 12 and 24 hr (Figure S3F). Importantly we observed that efficient sgRNA induction can be achieved with 10-fold-lower dox concentrations, and we only saw a drop in this induction when using 1,000-fold-less dox. To also validate the tightness of our system in vivo, we compared the engraftment efficiency and tumor burden in the NSG mice, which were subcutaneously injected with responder and non-responder cells (Figures S3G and S3H). Importantly, we observed that in the absence of dox, the BL clones, which are highly sensitive to induction of the *isgMcl-1*, could engraft as readily as the non-responder BL clones, indicating that the inducible CRISPR/Cas9 system remains tight in vivo.

Collectively, these findings demonstrate the tightness and high efficiency of our inducible CRISPR/Cas9 genome-editing system both in vitro and in vivo, and this can be attributed to the strong inducibility of the sgRNA driven by the H1 promoter. Therefore, we are able to use this lentiviral platform to even inactivate genes that are essential for the sustained growth of the targeted cells.

Generation of Hematopoietic-Cell-Restricted p53-Knockout/Mutant Mice

Next, we used our inducible CRISPR/Cas9 lentiviral platform for the rapid generation of mice lacking a gene/protein specifically in the hematopoietic compartment. Loss of one allele of *Trp53* (*Trp53*$^{+/-}$) markedly accelerates lymphoma development in *Eμ-Myc* transgenic mice (Schmitt et al., 1999; Michalak et al., 2009). Therefore, to test our platform in primary cells in vivo, we transduced fetal-liver-derived HSPCs from *Eμ-Myc* mice with sgRNAs targeting sequences in exon 4 or exon 5 of the *Trp53* gene (*jsgTrp53*) and transplanted these cells into lethally irradiated C57BL/6J-Ly5.1 congenic recipient mice that were then monitored for lymphoma development (Figure 4A). In order to delete/mutate the *Trp53* gene, we treated the transduced fetal liver cells and the hematopoietic-system-reconstituted mice with dox. All of these animals rapidly developed pre-B/B cell lymphoma (median latency of 29 days, with 100% incidence by 37 days; Figure 4B). In contrast, all mice transplanted with control sgRNA transduced *Eμ-Myc* transgenic HSPCs were still alive 100 days after reconstitution ($p < 0.0001$). DNA sequence analysis of lymphomas revealed that the acceleration in tumor development was due to targeting of both alleles of *Trp53* (Figures S4A and S4B). Accordingly, acceleration of tumor development was more rapid than that previously reported for loss of one *Trp53* allele (i.e., 100% incidence of lymphomas by ~70 days in *Eμ-Myc*;*Trp53*$^{+/-}$ mice) (Schmitt et al., 1999; Michalak et al., 2009). Notably, there was an increased proportion of surface immunoglobulin-M-positive lymphomas (88.2%) as compared with control *Eμ-Myc* mice (30%–40%) (data not shown), similar to that previously reported for *Eμ-Myc*;*Trp53*$^{+/-}$ mice (Michalak et al., 2009). The lymphomas that had been accelerated by the *jsgTrp53* sgRNA were resistant to apoptosis induced by the DNA-damaging agent, etoposide, confirming that they were functionally *Trp53* deficient (Figure 4C). Western blot analysis demonstrated that some of these lymphomas completely lacked TRP53 protein (Figure 4D), even after treatment with the *Trp53*-inducing drug etoposide (Figure 4E). Interestingly, other lymphomas displayed abnormally increased basal levels of TRP53 protein, as seen in in human as well as murine cancers carrying mutant *Trp53* (Freed-Pastor and Prives, 2012). The findings from the DNA sequence analysis and western blot analyses are summarized in Figure 4F. Of note, in some lymphomas that lack TRP53 protein, no *Trp53* gene mutations were detected using the NGS platform. This is likely due to the occurrence of large deletions that alter the PCR product or disrupt the primer binding sites. For example, lymphoma #53 only demonstrated one mutant *Trp53* allele; however, a truncated TRP53 protein was evident by western blotting (Figure 4D), indicative of a large deletion within the second *Trp53* allele. Interestingly, we again found that many independent lymphomas contained related InDel mutations generated by the *isgTrp53* (Figures S4A and S4B), similar to our findings with the *isgMcl-1*. The generation of stabilized, overexpressed mutant trp53 proteins in the lymphoma setting demonstrates that our inducible CRISPR/Cas9 systems offers an attractive approach to screen for novel tumor-promoting gain- or loss-of-function mutations in other oncogenes or tumor-suppressor genes, respectively.

DISCUSSION

The use of viral vectors carrying a drug-inducible sgRNA to elicit Cas9-mediated mutations in genes of interest provides a new versatility to the use of this exciting technology. We demonstrate the broad applicability of this system by knocking out or mutating genes in cells from different species both in vitro and in vivo. Temporal control of sgRNA activity allowed for high-efficiency CRISPR/Cas9-induced NHEJ repair. Importantly, this enabled the deletion of genes that are essential for sustained cell survival and growth in vitro and, excitingly, in a human xenograft model in vivo, showing the potential use of CRISPR/Cas9 in cancer therapy.

Recently, two dox-inducible Cas9 approaches have been proposed for the conditional deletion of genes. However, one of these studies never actually used the inducible nature of their Cas9 expression system to conditionally delete genes (Wang et al., 2014), and the application of the other was restricted to one cell type only (González et al., 2014). Importantly, neither of these studies reported the conditional deletion of genes that are essential for sustained cell growth. We also tested a dox-inducible Cas9 lentiviral vector, but we were unable to achieve the robust effects observed with the ubiquitously

(C) Functional validation of *Bim* deletion. BL cells were treated with ionomycin (5 μg/ml) for 72 hr, and cell viability was assessed by exclusion of PI measured in a flow cytometer. Data represent mean ± SEM.

(D) Read sequences obtained for human *Bim* exon 3 sgRNA targeted alleles in the Rael-BL cell line after treatment with dox. Wild-type *Bim* sequence is shown in the top line. DNA sequence changes are highlighted in red.

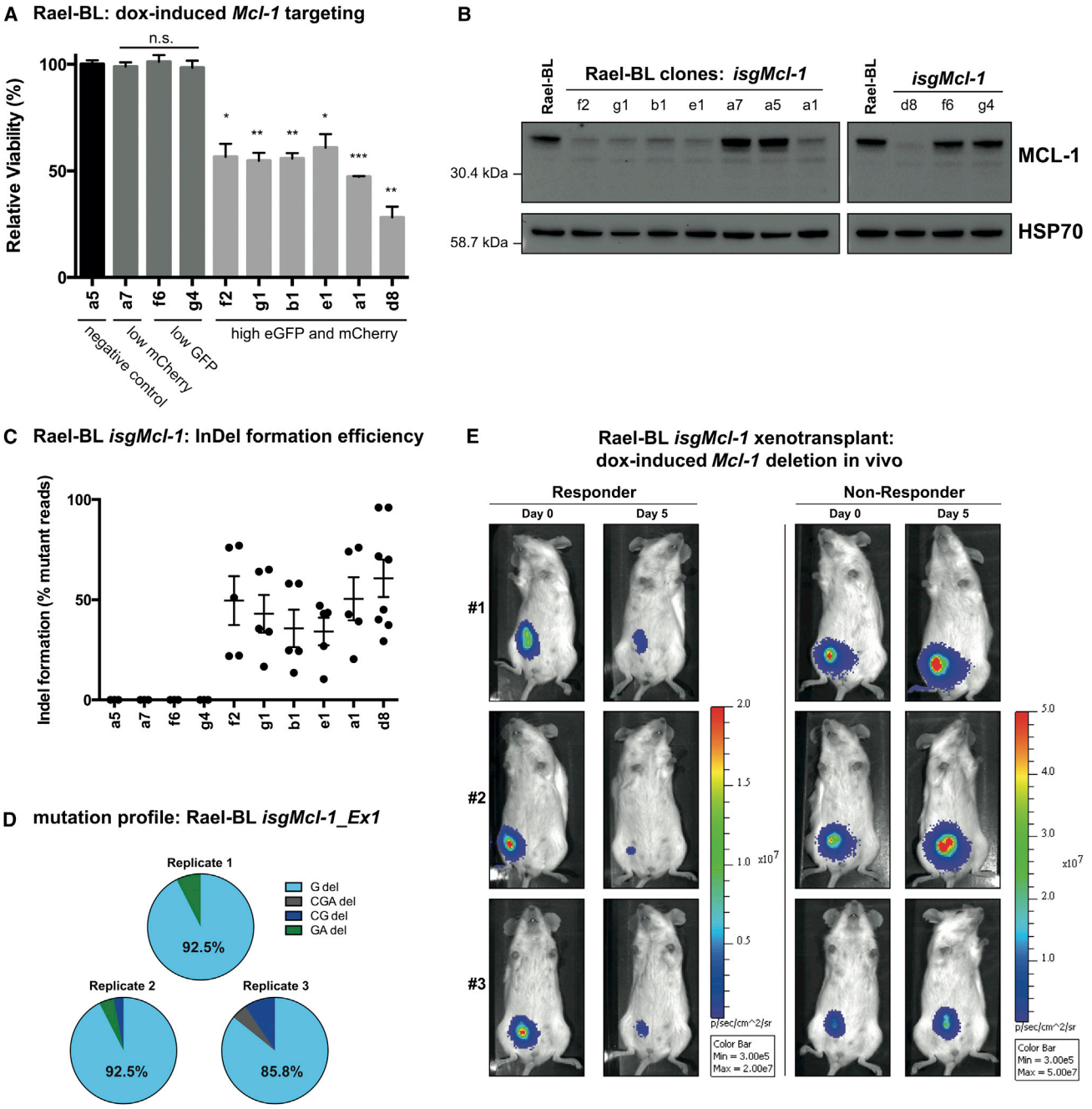

Figure 3. Inducible Deletion of the Essential Gene, *Mcl-1*, in a Human BL Cell Line with Assessment of Functional Consequences and Identification of Reoccurring Mutations

(A) Cas9-mediated loss of MCL-1 protein following induction of the *Mcl-1* sgRNA by dox leads to apoptosis in a bulk population of MCL-1-dependent human Burkitt lymphoma (BL) cell lines. Cell viability was assessed by exclusion of PI measured in a flow cytometer. Data represent mean ± SEM and are shown relative to the negative control (Cas9 negative) *$p < 0.05$, **$p < 0.01$, ***$p < 0.005$.

(B) Western blotting for MCL-1 (probing for HSP70 used as a loading control) shows efficient MCL-1 depletion following dox treatment in the presence of QVD-OPH (a broad-spectrum caspase inhibitor to prevent apoptosis and consequent protein degradation).

(C) NHEJ efficiency as calculated from percentage of mutant *Mcl-1* reads from analysis of MiSeq using the NGS platform as described. Individual values are shown with mean ± SEM (range across all samples, 13.5% to 96%).

(D) Mutational profile for *isgMcl1_huEx1* in the d8 Rael-BL cell line clone whole population after treatment with dox in three independent experiments demonstrating the presence of dominant and re-occurring mutations.

(legend continued on next page)

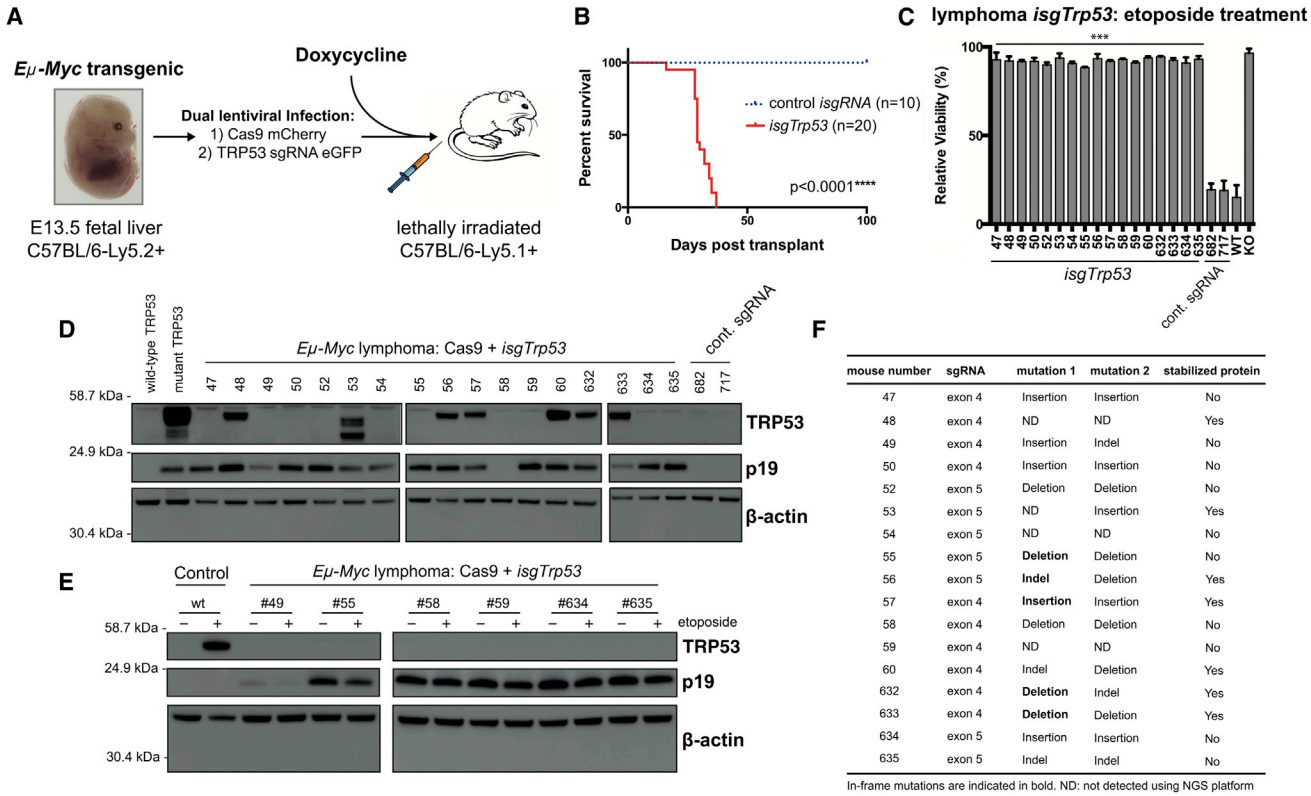

F

mouse number	sgRNA	mutation 1	mutation 2	stabilized protein
47	exon 4	Insertion	Insertion	No
48	exon 4	ND	ND	Yes
49	exon 4	Insertion	Indel	No
50	exon 4	Insertion	Insertion	No
52	exon 5	Deletion	Deletion	No
53	exon 5	ND	Insertion	Yes
54	exon 5	ND	ND	No
55	exon 5	**Deletion**	Deletion	No
56	exon 5	**Indel**	Deletion	Yes
57	exon 4	**Insertion**	Insertion	Yes
58	exon 4	Deletion	Deletion	No
59	exon 4	ND	ND	No
60	exon 4	Indel	Deletion	Yes
632	exon 4	**Deletion**	Indel	Yes
633	exon 4	**Deletion**	Deletion	Yes
634	exon 5	Insertion	Insertion	No
635	exon 5	Indel	Indel	No

In-frame mutations are indicated in bold. ND: not detected using NGS platform

Figure 4. CRISPR/Cas9-Mediated *Trp53*-Knockout/Mutation in *Eμ-Myc* Transgenic Mouse Hematopoietic Stem/Progenitor Cells Accelerates Lymphoma Development In Vivo

(A) Schematic for experimental design. HSPCs were obtained from the fetal liver of E13.5 C57BL/6J-Ly5.2$^+$ mice and maintained in vitro during dual lentiviral transduction with vectors encoding constitutive Cas9 and the inducible sgRNA. Cells were then injected into lethally irradiated congenic C57BL/6J-Ly5.1$^+$ recipient mice.

(B) Kaplan-Meier survival curve for mice reconstituted with *Eμ-Myc* HSPCs transduced with *Trp53*-targeting sgRNA compared to mice reconstituted with *Eμ-Myc* HSPCs transduced with a control sgRNA. The total number of mice (n) in each group is indicated. Median survival for the *isgTrp53* cohort is 29 days. ****p < 0.0001 for *isgTrp53* mice as compared to control sgRNA mice by log-rank analysis.

(C) Functional *Trp53* status was assessed by response of lymphoma cells to etoposide (0.05 μg/ml for 24 hr) treatment in vitro. Cell death was assessed by exclusion of PI measured in a flow cytometer. Data represent mean ± SEM; ***p < 0.001.

(D) Western blot analysis of each lymphoma for TRP53 protein and p19 with probing for β-actin used as a loading control. 41.2% of *Eμ-Myc isgTrp53* tumors assessed display abnormally high (stabilized) TRP53 protein, indicative of mutations in *Trp53*.

(E) Western blot analysis of lymphomas before and after treatment with etoposide (0.5 μg/ml for 24 hr) in the presence of the broad-spectrum caspase inhibitor QVD-OPH (25 μM) to prevent apoptosis.

(F) Table summary for CRISPR/Cas9-mediated *Trp53* mutations in lymphomas from selected mice. Mutations leading to in-frame sequence changes are shown in bold. All in-frame deletions and missense mutations resulting in stabilized overexpressed mutant TRP53 protein are accompanied by non-sense mutations.

expressed and strong H1 promoter (Ranganathan et al., 2014) (Figure S1). Importantly, we found that our system is very tight, showing almost no leakiness prior to the addition of dox in vitro and in vivo (Figures S1 and S3E–S3H). This is not only important for the deletion of essential genes but also critical to limit potential off-target effects, as Cas9 only becomes functional during the period of dox-induced sgRNA expression.

We have demonstrated the efficacy of our novel system in both human and mouse cell lines in vitro, in primary murine hematopoietic cells in an in vivo reconstitution model, and, most excitingly, in a human BL xenograft model in vivo. In contrast to the previously reported dox-inducible Pol-II systems (Ottina et al., 2012; González et al., 2014), we achieved high-efficiency induction as evidenced by robust mutation/knockout rates and impairment of tumor growth. Recently, an improved inducible RNAi platform has been developed, which also allows for efficient knockdown of a diverse set of genes (Fellmann et al., 2013). Unlike conventional CRISPR/Cas9-mediated

(E) BL mouse xenograft model to assess lymphoma progression and response to CRISPR/Cas9-mediated deletion of *Mcl-1 in vivo*. Bioluminescent imaging was performed prior (day 0) and 5 days after (day 5) continuous oral administration of dox. Shown are the three out of eight mice transplanted with responder clones that displayed the greatest impact of dox-induced *Mcl-1* deletion on tumor growth (responders, left panel). All mice bearing non-responder BL clones displayed marked tumor progression after dox treatment (non-responders, right panel). Color scale ranges for total photon flux are indicated.

gene targeting, RNAi is reversible, thereby allowing the re-expression of a suppressed gene. This might be of interest for some experimental settings, where consequences of transient suppression of gene function are desired.

Interestingly, we identified similar mutations induced by the NHEJ process from individual guide RNAs, even between different cell populations and experiments, both in vitro and in vivo. What is the reason for this unexpectedly low level of variation? One explanation could be that the NHEJ repair mechanism uses short sequence homologies for the joining reaction, thereby reducing the diversity of mutations (Roth and Wilson, 1986). An alternative explanation could be that the requirement of the proto-spacer-associated motive (PAM) site for Cas9 recognition and the cleavage site three bases upstream of the PAM site generate a "DNA environment" that is always repaired in a similar way. Since this has not been reported before, further investigations are required to elucidate the precise nature of the NHEJ DNA repair mechanism following CRISPR/Cas9-mediated double-strand breaks. This might provide useful information for designing more powerful sgRNAs to achieve specific knockin mutations without the requirement of a template DNA for homology-directed repair within the targeted genomic locus.

Finally, we have used our novel lentiviral platform to induce mutations in the tumor-suppressor gene *Trp53* in primary HSPCs, which were then used to reconstitute lethally irradiated mice. Surprisingly, we obtained different mutants of the TRP53 tumor suppressor that could all accelerate MYC-driven lymphoma development. This observation suggests that our CRISPR/Cas9 system can be adapted for the identification of novel mutations in oncogenes and tumor-suppressor genes that can initiate or accelerate tumor development.

EXPERIMENTAL PROCEDURES

Lentiviral Constructs

For the inducible sgRNA constructs, the previously described pFH1tUTG (Herold et al., 2008) plasmid was modified to contain the H1-Tet-sgRNA cassette, which was inserted into Pac I sites upstream of the hUbiquitin promoter. This sequence contains two bi-directional Bsmb1 sites for subsequent cloning of different sgRNA sequences. The constitutive sgRNA and Cas9 expression vectors were derived from the pFUGW, which has been described previously (Lois et al., 2002). For the constitutive sgRNA expression, the H1t promoter was inserted into the Pac1 site upstream of the hUbiquitin promoter. For the Cas9 expression vector, the eGFP cassette was replaced by the recently described Cas9 (Cong et al., 2013) linked via the T2A peptide to the mCherry fluorescent reporter protein. The lentiviral luciferase vector used for transducing the *isgMcl-1* BL cell lines has been recently described (Kelly et al., 2014).

sgRNA Design and Expression Analysis

The MIT CRISPR design software was used for the design of sgRNAs (http://crispr.mit.edu). To clone individual sgRNAs, 24-bp oligonucleotides containing the sgRNA sequences were synthesized (Geneworks). They included a 4-bp overhang for the forward (TCCC) and complementary reverse (AAAC) oligos to enable cloning into the Bsmb-I site of the lentiviral construct. sgRNA sequences are as follows: *Trp53* exon 4: 5′-GGCAACTATGGCTTCCACCT-3′; *Trp53* exon 5: 5′-GAGCGCTGCTCCGATGGTGA; *mBim* exon 2: 5′-GACA ATTGCAGCCTGCTGAG; *mBim* exon 3: 5′-GCACAGGAGCTGCGGCGGAT; *hBim* exon 2: 5′-GCCTCCCCAGCTCAGACCTG; *hBim* exon 3: 5′-GCCCAA GAGTTGCGGCGTAT; *hMcl1* exon 1.1: 5′-GGAGCTGGACGGGTACGAGC; *hMcl1* exon 1.2: 5′-GGGAGGGCGACTTTTGGCTA.

To analyze the sgRNA expression, RNA was first extracted with RNeasy mini columns (QIAGEN 74104) and 1 μg of extracted RNA was used for reverse transcription and first-strand cDNA synthesis. 2 μM of primer (5′-AAAAG CACCGACTCGGTGCC-3′) specific for the common 3′ scaffold sequence of sgRNAs was added to each reverse transcription reaction along with dinucleotide triphosphates, RNase inhibitor, and SuperScript III reverse transcriptase. Reactions were incubated for 1 hr at 50°C. For quantification of sgRNA cDNA sequences, TaqMan qPCR was conducted using forward primer (5′-CGGTAATCGGACTCAACCTCTA-3′), reverse primer (5′-CGCTTCCGCCAAT CACC 3′), and FAM-labeled TaqMan probe (5′ TTTGGCTACGGAGAAGGA GGCC 3′).

Tissue Culture

The mouse FDC-P1 cell line was grown in high-glucose DMEM supplemented with 10% fetal calf serum (FCS) (Gibco), 50 μM mercaptoethanol (Sigma-Aldrich), 100 μM asparagine (Sigma-Aldrich), 100 U/ml penicillin, 100 mg/ml streptomycin (Gibco), and IL-3 (10 ng/ml) at 37°C in 10% CO_2. HEK293T cells were maintained in DMEM with 10% FCS. Prior to transfection, HEK293T cells were cultured in DME Glutamax (Gibco) supplemented with 10% FCS and 25 mM HEPES. Rael-BL, Kem-BL, and Sal-BL human-BL-derived cell lines have been described previously (Kelly et al., 2002). These cell lines were cultured in RPMI-1640 supplemented with 10% FCS, 1 mM glutamine (Gibco), 1 mM sodium pyruvate (Gibco) and 50 μM thioglycerol (Sigma-Aldrich), maintained in 5% CO_2.

Virus Production and Transduction of Cell Lines

Lentiviral particles were produced by transient transfection of 293T cells grown in 10-cm Petri dishes with 10 μg of vector DNA along with the packaging constructs pMDL (5 μg), pRSV-rev (2.5 μg), and either pENV (5 μg) (for fetal liver cell infections) or pVSV-G (3 μg) (for cell line infections) using standard calcium phosphate precipitation as previously described (Herold et al., 2008). Virus-containing supernatants were collected at 48–72 hr after transfection and passed through a 0.45-μm filter. For infection of 293T cells, cells were plated at 1×10^4 cells per 12-well plate in 1-ml viral supernatant plus 1 ml DMEM with 10% FCS; cells were left for 72 hr. For mouse FDC-P1 and human BL cell lines, aliquots of 1.0×10^5 cells were suspended in 8 ml of virus-containing supernatant with 10 ng/μl polybrene, incubated for 30 min at 37°C, and then centrifuged at 2,200 rpm for 2.5 hr at 32°C.

Flow Cytometric Analysis and Cell Sorting

Assessment of eGFP and mCherry expression in cell lines as well as immunophenotyping of *Eμ-Myc* lymphomas was performed using an LSR IIW or FACSCalibur flow cytometer (Becton Dickinson). Immunophenotyping of *Eμ-Myc* lymphomas was performed on single-cell suspensions that were stained with surface-marker-specific antibodies. The following fluorochrome-conjugated antibodies were utilized: CD19 (clone ID3), B220 (RA3-6B2), IgM (clone 5.1), IgD (clone 11-26C), CD4 (clone H129), CD8 (clone YTS.169), Mac-1 (clone M1/70) and Gr-1 (clone RB6-8C5). To confirm the lymphomas were of donor hematopoietic cell derived origin, staining for Ly5.2 was also performed. Antibodies were produced in our laboratory and conjugated to R-phycoerythrin (R-PE) or allophycocyanin according to the manufacturer's instructions. Virally transduced cell lines were sorted using an Aria W flow cytometer by two methods: (1) all cells positive for eGFP and mCherry were sorted to produce a bulk population of double-positive cells (referred to as a whole population), or (2) dual-positive eGFP and mCherry cells were sorted on a single-cell basis into a single well of a 96-well plate to propagate a homogenous cell population (referred to as single-cell clones).

Dox Treatment

For treatment of cell lines to induce expression of the sgRNA, dox hyclate (Sigma-Aldrich D9891) was dissolved in sterile water at a stock concentration of 10 mg/ml and added to tissue culture medium for a final concentration of 1 μg/ml. For in vivo experiments, standard rodent diet was supplemented with dox 600 mg/kg body weight (Specialty Feeds, SF08-026).

Drug Treatments and Functional Assays

The viability of cultured cells was determined by exclusion of propidium iodide (PI) as assessed by flow cytometry. PI-negative cells were considered viable, and this was expressed as a percentage of the viability of a matched untreated

control cell population. Single-cell clones were obtained for Rael-BL and Kem-BL cell lines transduced with both *isgBim* and Cas9. Tissue culture medium was supplemented with 5 μg/ml ionomycin, and cell viability was assessed by exclusion of PI after 72 hr. Single-cell clones were obtained for Rael-BL clones transduced with both *isgMcl-1* and Cas9. At commencement of functional assays, the tissue culture medium was supplemented with 1 μg/ml dox to induce the *isgMcl-1* in the entire cell population. Cell viability was assessed after 72 hr, at which time point samples for analyses of genomic DNA and protein (western blotting) were also collected. To assess the TRP53 functional status of the *isgTrp53 Eμ-Myc* lymphomas, cell lines derived from these tumors were treated in vitro with etoposide 0.05 μg/ml and cell viability assessed by exclusion of PI after 24 hr.

Western Blot Analysis

Total protein extracts were prepared from cell lines and primary tumor samples by lysis in RIPA buffer supplemented with protease inhibitors (complete protease inhibitor cocktail, Roche). Protein extracts were quantitated using the Bradford assay (Bio-Rad). Total protein extracts were separated by SDS-PAGE and transferred onto nitrocellulose membranes. Membranes were blocked using 5% milk in PBS with 0.1% Tween 20 prior to incubation with the primary antibody. Polyclonal antibodies were used to detect mouse MCL-1 (Rockland antibodies and assays), and BIM (Enzo Life Sciences, ADI-AAP-330-E); monoclonal antibodies were used to detect mouse TRP53 (CM5, Novocastra), p19/ARF (clone 5.C3.1, Rockland Antibodies and Assays), β-actin (clone AC74, Sigma-Aldrich; loading control), HSP70 (clone N6; gift from Dr. R. Anderson, Peter MacCallum Cancer Research Institute, Melbourne, Australia; loading control), human MCL-1 (clone 19C4-15) and Cas9 (Diagenode, #C15200203). Etoposide treatment of *Eμ-Myc* lymphoma cells was performed in vitro using etoposide (0.5 μg/ml) in the presence of the broad-spectrum caspase inhibitor QVD-OPH (MP Biomedicals, cat#OPH109) to prevent cell death and associated protein degradation. Cells were plated at 5×10^5 cells per 24-well plate, and protein extracts were obtained after 24 hr.

Animal Experiments

Experiments with mice were conducted according to the guidelines of the Walter and Eliza Hall Institute animal ethics committee. *Eμ-Myc* transgenic mice (C57BL/6J) have been described previously (Adams et al., 1985). CRISPR/Cas9 *Bim* mutant mice (C57Bl/6J) were generated as described before (Wang et al., 2013). For the human xenograft experiments, 1×10^6 luciferase-transduced BL cell lines were injected into NSG mice. After 21 days, the tumor burden was visualized using bioluminescent imaging. Prior to imaging, mice were administered with 200 μl of 15-mg/ml D-luciferin potassium salt (Caliper Life Sciences) in PBS by intraperitoneal (i.p.) injection. Mice were then anaesthetized using isoflurane inhalant and imaged using the IVIS live-imaging system (Perkin Elmer) to detect luciferase bioluminescence exactly 15 min after administration of the luciferin substrate. The tumor burden was quantified by measuring the total photon flux per second emitted from a region of interest drawn around the whole mouse. When the lymphoma burden was sufficiently high (photon flux per second of $>1 \times 10^7$), successfully engrafted mice from each cohort were administered dox-containing food for 5 days and regression or progression was assessed by repeat bioluminescence imaging. For hematopoietic reconstitutions, fresh embryonic day 13.5 (E13.5) fetal liver cells (a rich source of HSPCs) were obtained from C57BL/6J-Ly5.2$^+$ mice and placed into alpha-minimum essential medium (α-MEM) with glutamax (Gibco) supplemented with 10% FCS, 1 mM L-glutamine, 1 mM sodium pyruvate, 100 μg/ml streptomycin, 100 U/ml penicillin, 10 mM HEPES, 50 μM β-mercaptoethanol containing the cytokines IL-6 (10 ng/ml), stem cell factor (100 ng/ml), thrombopoietin (50 ng/ml) and FLT-3 ligand (10 ng/ml). Fetal liver cells were maintained in culture for approximately 72 hr during lentiviral infection. Dual lentiviral infection was performed with (1) constitutive Cas9-mCherry and (2) dox-inducible sgRNA-eGFP lentivirus. Viral supernatants were collected as described above, and 10 ng/μl polybrene was added. Viral supernatants were combined at a ratio of three parts Cas9 virus to two parts sgRNA virus to allow simultaneous infection. Infections were performed in a 6-well non-tissue-culture-treated plate previously coated overnight with retronectin solution (32 μg/ml in PBS) at 4°C followed by coating with 2% albumin solution from bovine serum (Sigma-Aldrich A1595) in PBS at 37°C for 30 min prior to coating with viral particles. Viral particles were centrifuged onto the retronectin-coated plates at 3,500 rpm for 1 hr. Fetal liver cells were then added to each well and incubated for 24 hr. A second round of lentiviral infection was performed on day 2, at which time medium was also supplemented with 1 μg/ml dox. Transduced cells were collected, washed in PBS, and injected into lethally irradiated (2 × 5.5Gy, 4 hr apart) C57BL/6J-Ly5.1$^+$ mice. Recipient mice were maintained on dox-containing food during the period of reconstitution.

Statistical Analysis

GraphPad Prism software was used for generating Kaplan-Meier animal survival curves and statistical analysis comparing survival curves by log-rank test. GraphPad software was also used in the analysis of death assays with etoposide-, ionomycin-, and dox-induced *Mcl-1* deletion. Paired two-tailed t tests were performed to compare samples.

Sanger Sequencing of sgRNA Target Sites

Genomic DNA was isolated from cells using the DNeasy kit (QIAGEN). PCR using AccuPrime (Invitrogen) was performed using primers flanking the target sites for the human and mouse *Bim* sgRNAs (primer numbers: 369 370 [mouse]). PCR products were blunt-end ligated into plasmids using the Zero Blunt TOPO PCR Cloning Kit (Invitrogen). Plasmids were transformed by electroporation into DH10α-competent bacteria (Invitrogen). Single bacterial colonies were grown in Luria broth supplemented with kanamycin, and plasmid DNA was purified by standard mini-prep protocol. DNA sequencing was performed by conventional Sanger sequencing (Australian Genome Research Facility). For FDC-P1 cell lines, genomic DNA was obtained from single-cell clones. For 293T cells, genomic DNA was obtained from whole populations of cells.

Targeted PCR of Sites of Cas9-Induced InDels

Preparation of genomic DNA was performed by placing cells directly into Direct PCR lysis buffer (Viagen) with proteinase K (Sigma-Aldrich P4850) and incubated at 56°C for 4 hr followed by heat inactivation at 85°C for 40 min. Unique primers were designed to span the expected InDel positions in the genomic DNA, such that approximately 120 bp of DNA sequence 5′ and 3′ of predicted Cas9-mediated double-strand breaks would be amplified during the first PCR reaction. The amplicon size range generated was 200-300 bp so that these fragments could be sequenced using the Illumina MiSeq platform. The unique primers were synthesized to include a 22 and 21 base overhang at the 5′ end of the forward and reverse primers, respectively (OH1: 5′-GTGACCTATGAACTCAGGAGTC-3′; OH2: 5′-CTGAGACTTGCAC ATCGCAGC-3′). The PCR cycling conditions were as follows (PCR 1: 95°C 2 min [95°C 15 s, 60°C 15 s, 72°C 30 s] × 18, 72°C 7 min, 4°C hold step). PCR amplicons were individually purified using 1.0× Ampure Beads (Beckman Coulter). Amplicon size distribution was ascertained using the Agilent Tapestation D1000 protocol.

Secondary Amplification using Overhang Sequences

In order to maximize sample sequencing on the Illumina MiSeq platform, individual amplicon identification was devised using eight base index sequences derived from the Illumina Nextera design. This approach ensured that the required sequences (flow-cell binding and sequencing primers) for Illumina sequencing technology were incorporated into PCR amplicons generated during the primary amplification step, during the following secondary overhang amplification step. Eight forward index primers and 12 reverse index primers were designed for use in a 96-well plate format. (SRT1_OH1: 5′- CAAGCA GAAGACGGCATACGAGATCCGGTCTCGGCATTCCTGCTGAACCGCTCTTC CGATCTNNNNNNNNGTGACCTATGAACTCAGGAGTC-3′; SRT2-OH2: 5′-AATGATACGGCGACCACCGAGATCTACACTCTTTCCCTACACGACGCTCT TCCGATCTNNNNNNNNCTGAGACTTGCACATCGCAGC-3′. The sequence NNNNNNNN is where individual indexes are placed in the oligo design.)

The PCR cycling conditions were as follows (PCR 2: 95°C for 2 min [95°C for 15 s, 60°C for 15 s, 72°C for 30 s] × 24, 72°C for 7 min, 4°C hold step). Amplicon size distribution was ascertained using the Agilent Tapestation D1000 protocol. The 96 reactions from the entire plate were pooled and the PCR amplicons purified using 1.0× Ampure Beads (Beckman Coulter).

Illumina MiSeq Sequencing

Each dual indexed library plate pool was quantified using the Agilent Tapestation and the Qubit RNA assay kit for Qubit 2.0 Fluorometer (Life Technologies). The indexed pool was diluted to 12 pM for sequencing on a MiSeq instrument (Illumina) according to the manufacturer's instructions. The 300-cycle kit was used for amplicon sizes of less than 280 bp, and these amplicons were sequenced as single reads (281 cycles) followed by a 44-cycle second index read. Amplicons that were larger than 280 bp were sequenced using the 600-cycle kit, and both reads 1 and 2 were sequenced for 311 cycles.

SUPPLEMENTAL INFORMATION

Supplemental Information includes four figures and can be found with this article online at http://dx.doi.org/10.1016/j.celrep.2015.02.002.

AUTHOR CONTRIBUTIONS

B.J.A., G.L.K., A.S., and M.J.H. wrote the manuscript and designed experiments. G.L.K., B.J.A., M.S.B., L.T., A.J. K., A.S., L.O., L.M., S.W., and M.J.H. performed and analyzed the experiments.

ACKNOWLEDGMENTS

We thank all members of the M.J.H. laboratory for their support and advice; D. Gray for critical reading of the manuscript; G. Siciliano, C. Gatt, and their team for animal husbandry; S. Monard and his team for help with the flow cytometry unit; A.B. Rickinson and M. Rowe (University of Birmingham) for the kind gift of BL cell lines; and K. Rogers and the WEHI imaging facility. This work was supported by a Leukemia Foundation National Research Program Clinical PhD Scholarship (to B.J.A.), a Kay Kendall Leukemia Fund Intermediate Fellowship (KKL331 to G.L.K.); the National Health and Medical Research Council, Australia program grant 1016701 and fellowship 1020363, Leukemia and Lymphoma Society SCOR grant 7001-13 (to A.S.), and project grant GNT1049720 (to M.J.H.). This work was made possible through Victorian State Government Operational Infrastructure Support and Australian Government National Health and Medical Research Council Independent Research Institutes Infrastructure Support Scheme.

Received: October 1, 2014
Revised: December 15, 2014
Accepted: January 29, 2015
Published: February 26, 2015

REFERENCES

Adams, J.M., Harris, A.W., Pinkert, C.A., Corcoran, L.M., Alexander, W.S., Cory, S., Palmiter, R.D., and Brinster, R.L. (1985). The c-myc oncogene driven by immunoglobulin enhancers induces lymphoid malignancy in transgenic mice. Nature *318*, 533–538.

Barrangou, R., Fremaux, C., Deveau, H., Richards, M., Boyaval, P., Moineau, S., Romero, D.A., and Horvath, P. (2007). CRISPR provides acquired resistance against viruses in prokaryotes. Science *315*, 1709–1712.

Bouillet, P., Metcalf, D., Huang, D.C.S., Tarlinton, D.M., Kay, T.W.H., Köntgen, F., Adams, J.M., and Strasser, A. (1999). Proapoptotic Bcl-2 relative Bim required for certain apoptotic responses, leukocyte homeostasis, and to preclude autoimmunity. Science *286*, 1735–1738.

Cong, L., Ran, F.A., Cox, D., Lin, S., Barretto, R., Habib, N., Hsu, P.D., Wu, X., Jiang, W., Marraffini, L.A., and Zhang, F. (2013). Multiplex genome engineering using CRISPR/Cas systems. Science *339*, 819–823.

Fellmann, C., Hoffmann, T., Sridhar, V., Hopfgartner, B., Muhar, M., Roth, M., Lai, D.Y., Barbosa, I.A.M., Kwon, J.S., Guan, Y., et al. (2013). An optimized microRNA backbone for effective single-copy RNAi. Cell Rep. *5*, 1704–1713.

Fire, A., Xu, S., Montgomery, M.K., Kostas, S.A., Driver, S.E., and Mello, C.C. (1998). Potent and specific genetic interference by double-stranded RNA in Caenorhabditis elegans. Nature *391*, 806–811.

Freed-Pastor, W.A., and Prives, C. (2012). Mutant p53: one name, many proteins. Genes Dev. *26*, 1268–1286.

González, F., Zhu, Z., Shi, Z.D., Lelli, K., Verma, N., Li, Q.V., and Huangfu, D. (2014). An iCRISPR platform for rapid, multiplexable, and inducible genome editing in human pluripotent stem cells. Cell Stem Cell *15*, 215–226.

Herold, M.J., van den Brandt, J., Seibler, J., and Reichardt, H.M. (2008). Inducible and reversible gene silencing by stable integration of an shRNA-encoding lentivirus in transgenic rats. Proc. Natl. Acad. Sci. USA *105*, 18507–18512.

Jinek, M., Chylinski, K., Fonfara, I., Hauer, M., Doudna, J.A., and Charpentier, E. (2012). A programmable dual-RNA-guided DNA endonuclease in adaptive bacterial immunity. Science *337*, 816–821.

Jinek, M., Jiang, F., Taylor, D.W., Sternberg, S.H., Kaya, E., Ma, E., Anders, C., Hauer, M., Zhou, K., Lin, S., et al. (2014). Structures of Cas9 endonucleases reveal RNA-mediated conformational activation. Science *343*, 1247997.

Kelly, G., Bell, A., and Rickinson, A. (2002). Epstein-Barr virus-associated Burkitt lymphomagenesis selects for downregulation of the nuclear antigen EBNA2. Nat. Med. *8*, 1098–1104.

Kelly, G.L., Grabow, S., Glaser, S.P., Fitzsimmons, L., Aubrey, B.J., Okamoto, T., Valente, L.J., Robati, M., Tai, L., Fairlie, W.D., et al. (2014). Targeting of MCL-1 kills MYC-driven mouse and human lymphomas even when they bear mutations in p53. Genes Dev. *28*, 58–70.

Lois, C., Hong, E.J., Pease, S., Brown, E.J., and Baltimore, D. (2002). Germline transmission and tissue-specific expression of transgenes delivered by lentiviral vectors. Science *295*, 868–872.

Mali, P., Yang, L., Esvelt, K.M., Aach, J., Guell, M., DiCarlo, J.E., Norville, J.E., and Church, G.M. (2013). RNA-guided human genome engineering via Cas9. Science *339*, 823–826.

Michalak, E.M., Jansen, E.S., Happo, L., Cragg, M.S., Tai, L., Smyth, G.K., Strasser, A., Adams, J.M., and Scott, C.L. (2009). Puma and to a lesser extent Noxa are suppressors of Myc-induced lymphomagenesis. Cell Death Differ. *16*, 684–696.

Mizuno, T., Chou, M.Y., and Inouye, M. (1984). A unique mechanism regulating gene expression: translational inhibition by a complementary RNA transcript (micRNA). Proc. Natl. Acad. Sci. USA *81*, 1966–1970.

Ottina, E., Grespi, F., Tischner, D., Soratroi, C., Geley, S., Ploner, A., Reichardt, H.M., Villunger, A., and Herold, M.J. (2012). Targeting antiapoptotic A1/Bfl-1 by in vivo RNAi reveals multiple roles in leukocyte development in mice. Blood *119*, 6032–6042.

Pennisi, E. (2013). The CRISPR craze. Science *341*, 833–836.

Ranganathan, V., Wahlin, K., Maruotti, J., and Zack, D.J. (2014). Expansion of the CRISPR-Cas9 genome targeting space through the use of H1 promoter-expressed guide RNAs. Nat. Commun. *5*, 4516–4522.

Roth, D.B., and Wilson, J.H. (1986). Nonhomologous recombination in mammalian cells: role for short sequence homologies in the joining reaction. Mol. Cell. Biol. *6*, 4295–4304.

Schmitt, C.A., McCurrach, M.E., de Stanchina, E., Wallace-Brodeur, R.R., and Lowe, S.W. (1999). INK4a/ARF mutations accelerate lymphomagenesis and promote chemoresistance by disabling p53. Genes Dev. *13*, 2670–2677.

Sontheimer, E.J. (2005). Assembly and function of RNA silencing complexes. Nat. Rev. Mol. Cell Biol. *6*, 127–138.

Wang, H., Yang, H., Shivalila, C.S., Dawlaty, M.M., Cheng, A.W., Zhang, F., and Jaenisch, R. (2013). One-step generation of mice carrying mutations in multiple genes by CRISPR/Cas-mediated genome engineering. Cell *153*, 910–918.

Wang, T., Wei, J.J., Sabatini, D.M., and Lander, E.S. (2014). Genetic screens in human cells using the CRISPR-Cas9 system. Science *343*, 80–84.

Wiedenheft, B., Sternberg, S.H., and Doudna, J.A. (2012). RNA-guided genetic silencing systems in bacteria and archaea. Nature *482*, 331–338.